PASJ: Publ. Astron. Soc. Japan
© 2008. Astronomical Society of Japan.

arXiv:0707.2640v1 [astro-ph] 18 Jul 2007

Observations of B335 in the Millimeter Continuum and the 226 GHz H_2CO Line

Minho Choi
International Center for Astrophysics, Korea Astronomy and Space Science Institute, Hwaam 61-1, Yuseong, Daejeon 305-348, South Korea
minho@kasi.re.kr

(Received 2007 March 26; accepted 2007 July 15)

Abstract

The protostar B335 was observed in the 1.3 mm continuum and in the H_2CO $3_{12} \rightarrow 2_{11}$ line with an angular resolution of about $8''$. The mass of the inner envelope detected by the dust continuum emission is about 0.02 $M_\odot$. The H_2CO spectrum at the protostellar position shows a blue-skewed double peak profile, suggesting that the kinematics of the inner envelope is dominated by infall motion. When the blueshifted and the redshifted peaks were imaged separately, however, there is a small east-west displacement between the maximum positions. This displacement suggests that some part of the H_2CO emission might come from the outflowing gas. A combined effect of the infalling envelope and the outflow on the radiative transfer is discussed. This effect can make the line profile asymmetry severer than what is expected from infall-only models.

Key words: ISM: individual (B335) — ISM: structure — stars: formation

1. Introduction

B335 is an isolated globule at a distance of 250 pc from the Sun (Barnard 1927[1]; Bok et al. 1971; Bok & McCarthy 1974; Tomita et al. 1979; Frerking et al. 1987). In the dense core of B335, there is a low-luminosity (3 $L_\odot$) young stellar object detected in far-IR/submillimeter (Keene et al. 1983; Gee et al. 1985; Chandler et al. 1990). A compact source elongated roughly in the north-south direction was revealed by interferometric imaging of the millimeter continuum emission from dust (Hirano et al. 1992; Chandler & Sargent 1993; Choi et al. 1999; Wilner et al. 2000). B335 is an archetypical Class 0 source and considered as a protostar in the main accretion phase (André et al. 1993). It is one of the best studied protostars.

Early radio observations of B335 suggested that the 22 $M_\odot$ globule contains dense molecular gas (Minn & Greenberg 1973; Milman et al. 1975; Martin & Barrett 1978). Zhou et al. (1990) showed that the dense core has a steep density gradient. Star forming activities were revealed by molecular line observations (Frerking & Langer 1982; Frerking et al. 1987). CO line observations showed that there is a bipolar outflow oriented nearly in the plane of the sky with an opening angle of $\sim 50^\circ$ (Hirano et al. 1988; Cabrit et al. 1988). The outflow axis is in the east-west direction, and the millimeter continuum source is located between the two outflow lobes, which suggests that the protostar at the center of the dense core is driving the outflow (Hirano et al. 1992; Chandler & Sargent 1993; Choi et al. 1999). A compact radio thermal jet was detected near the protostellar position (Anglada et al. 1992; Reipurth et al. 2002). Herbig-Haro objects (HH 119) and shock-excited molecular hydrogen features were detected along the outflow axis (Reipurth et al. 1992; Hodapp 1998).

B335 is one of the first examples of protostars showing a spectroscopic signature of infall motion, i.e., blue-skewed double-peak line profiles. By comparing observations of several transitions of CS and H_2CO with synthetic spectra from radiative transfer calculations of self-similar collapse models, parameters of the collapsing envelope, such as infall radius and molecular abundances, were derived (Zhou et al. 1993; Choi et al. 1995). More detailed observations and modelings using high-density tracers and near-IR extinction maps provided a rich array of information on the protostellar collapse of B335 (Gregersen et al. 1997; Saito et al. 1999; Choi et al. 1999; Wilner et al. 2000; Harvey et al. 2001; Takakuwa et al. 2007). Interferometric observations of the millimeter continuum showed that the density gradient of the inner envelope has a power-law index of ~ 1.55, which is consistent with the theoretical expectations (1.5) of gravitational free fall (Harvey et al. 2003a, 2003b). Evans et al. (2005) presented chemical models by comparing observations of about 30 transitions with model spectra generated from calculations of dust radiative transfer, molecular line radiative transfer, and chemical evolutions. These observations and modelings collectively showed that B335 is probably the best object for the study of protostellar collapse and related phenomena, and it is important to collect more data in order to test our understanding of star formation at the earliest evolutionary stage.

This Letter presents observations of the B335 region in the λ = 1.3 mm continuum and the H_2CO line using the Berkeley-Illinois-Maryland Association (BIMA) array. In § 2 we describe our observations. In § 3 we report the results of the BIMA imaging and discuss the structure of the protostellar core.

2. Observations

The λ = 1.3 mm continuum and the H_2CO $3_{12} \rightarrow 2_{11}$ line (225.697772 GHz) were observed using the BIMA array in the D-array configuration on 1999 September 4. The phase tracking center was $\alpha_{2000} = 19^{\rm h}37^{\rm m}00\overset{\rm s}{.}99$ and $\delta_{2000} = 07^\circ34'10\overset{''}{.}8$.

---

[1] See http://www.library.gatech.edu/barnard/ and the Dark Objects Catalogue therein.

A narrow spectral window was used for the H_2CO line with a spectral resolution of 0.098 MHz giving a velocity resolution of 0.13 km s^{-1}. For the continuum, six wide spectral windows at each sideband were used, resulting in a single-sideband bandwidth of 600 MHz. These wide windows do not contain any strong line. The phase was determined by observing a nearby quasar 2013+370 (NVSS J201528+371059). The flux calibration was done by observing Uranus. Maps were made using a CLEAN algorithm. Natural weighting was used for all the images presented in this Letter.

3. Results and Discussion

3.1. *Millimeter Continuum*

The 1.3 mm continuum emission was detected in both the lower and the upper sidebands. Since combining the data of the two sidebands did not improve the signal-to-noise ratio, we present the map made using the lower sideband data only (Fig. 1). The peak flux density is 97 ± 19 mJy beam^{-1}, and the total flux is 180 ± 60 mJy. (The peak flux of the upper-sideband map is 70 ± 20 mJy beam^{-1}.) The 1.3 mm peak position is consistent with the millimeter/centimeter position of previously published maps (Wilner et al. 2000; Reipurth et al. 2002).

Figure 2 shows the spectral energy distribution of B335 in the millimeter-centimeter range. From the three data points in the millimeter band, the best-fit power-law spectrum has a spectral index of $\alpha \approx 2.3$, which suggests that the millimeter emission mostly comes from dust. For comparison, the spectral index in the submillimeter band within a 40″ aperture is 2.9 ± 0.6 (Shirley et al. 2000).

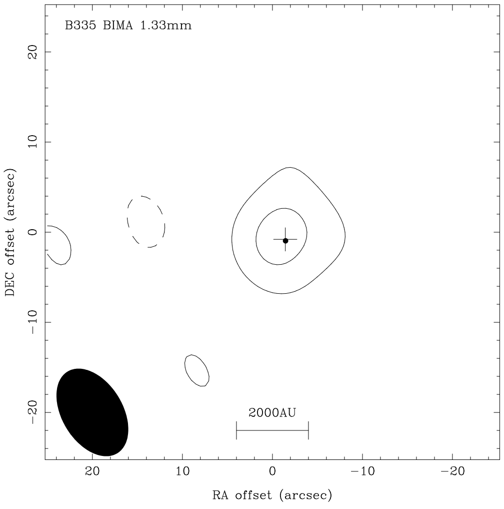

Fig. 1. Map of the λ = 1.3 mm continuum toward the B335 region. The contour levels are 40 and 80 mJy beam^{-1}. Dashed contours are for negative levels. The rms noise is 19 mJy beam^{-1}. Shown at the bottom left corner is the synthesized beam: FWHM = 10.″6 × 6.″7 and P.A. = 31°. The straight line at the bottom corresponds to 2000 AU at a distance of 250 pc. *Plus*: Position of the 1.2 mm continuum source (Wilner et al. 2000). *Filled circle*: Position of the 3.6 cm continuum source (Reipurth et al. 2002).

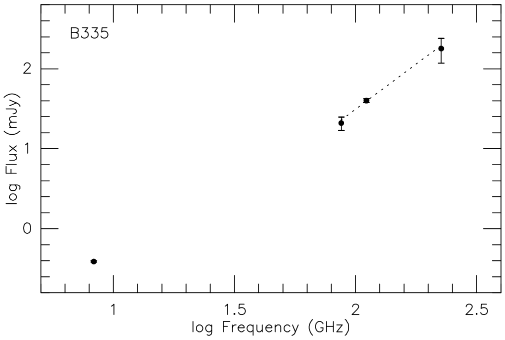

Fig. 2. Spectral energy distribution of B335 from interferometric observations. Flux densities are from Reipurth et al. (2002), Choi et al. (1999), Chandler & Sargent (1993), and this work. The flux density at λ = 3.4 mm from the data presented by Choi et al. (1999) is 21 ± 4 mJy. *Dotted straight line*: Best-fit power-law spectrum in the millimeter range. The spectral index is α = 2.3 ± 0.3.

To derive the mass from the dust continuum flux, the dust emissivity given by Beckwith & Sargent (1991) is assumed,

$$\kappa_\nu = 0.1 \left(\frac{\nu}{\nu_0}\right)^\beta \text{cm}^2\ \text{g}^{-1}, \tag{1}$$

where ν is the frequency, ν_0 = 1200 GHz, and β is the opacity index ($\beta \approx \alpha - 2$, in the millimeter range). If the emission is optically thin, the mass can be estimated by

$$M = \frac{F_\nu D^2}{\kappa_\nu B_\nu(T_d)}, \tag{2}$$

where F_ν is the flux density, D is the distance to the source, B_ν is the Planck function, and T_d is the dust temperature. Dust radiative transfer modelings show that the dust temperature within 0.006 pc (5″) from the center ranges from 20 K to ∼40 K (Evans et al. 2005). Assuming D = 250 pc and T_d = 30 ± 10 K, a rough estimate of the mass from the interferometric observations is M = $0.021^{+0.017}_{-0.007}$ $M_\odot$, which includes the inner protostellar envelope and the disk. The mass estimate is very sensitive to the opacity index, and Chandler & Sargent (1993) derived 0.21 $M_\odot$ by assuming β = 1.2. For comparison, the 1.3 mm flux density within a 40″ beam is 0.57 Jy, and the mass estimate within a 120″ beam is 1.2 $M_\odot$ (Shirley et al. 2000).

3.2. *The H_2CO Line*

Figure 3 shows the map of the H_2CO line integrated over the full width of the line. The strongest emission peak coincides with the central protostellar position. There is a secondary emission structure near the northwestern corner of the map, which is probably related with the outflow.

Figure 4 shows the H_2CO spectrum at the protostellar position. Similarly to most of the optically thick molecular lines seen toward B335, the H_2CO line also shows a blue-skewed double peak line profile that may be interpreted as a sign of infall motion. However, when the blueshifted and the redshifted peaks were imaged separately, there is a small east-west displacement between the maximum positions (Fig. 5). The spectra at the maximum positions are shown in Figure 6. Since the bipolar outflow is also in the east-west direction (Hirano et al. 1992), the displacement may be related with the outflow. That is, some part of the H_2CO emission might come from the outflowing gas. This contribution from the outflow may provide

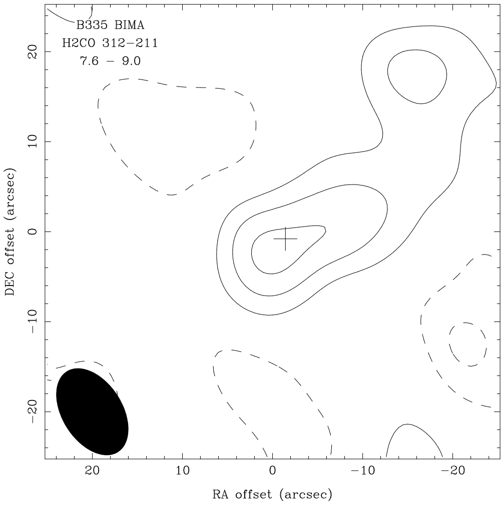

Fig. 3. Map of the H_2CO line toward the B335 region. The H_2CO line intensity was averaged over the velocity interval of $V_{\rm LSR}$ = (7.6, 9.0) km s^{-1}. The contour levels are 1, 2, and 3 times 0.7 Jy $beam^{-1}$. The rms noise is 0.26 Jy $beam^{-1}$. Shown at the bottom left corner is the synthesized beam: FWHM = $10\farcs6 \times 6\farcs7$ and P.A. = 32°. *Plus*: Position of the 1.2 mm continuum source (Wilner et al. 2000).

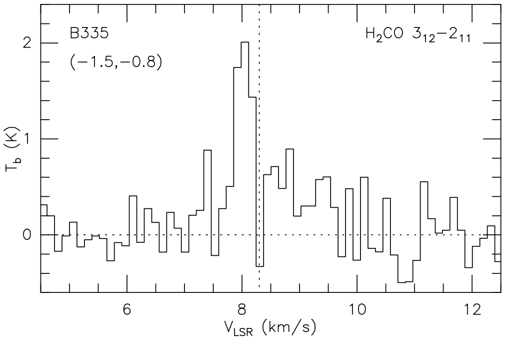

Fig. 4. Spectrum of the H_2CO line at the B335 protostellar position. *Vertical dotted line*: Systemic velocity of the B335 cloud core, based on the average of optically thin lines ($V_{\rm LSR}$ = 8.30 ± 0.05 km s^{-1}; Evans et al. 2005).

an explanation on the particularly poor fit of the H_2CO $3_{12} \rightarrow 2_{11}$ line in the modeling of line profiles (Zhou et al. 1993; Choi et al. 1995).

Wilner et al. (2000) arrived at a similar conclusion from interferometric observations of the CS $J = 5 \rightarrow 4$ line. The high-resolution CS maps are dominated by clumps aligned in the east-west direction, which was interpreted as a slow, dense component of the bipolar outflow. However, there is an interesting difference between the H_2CO and the CS maps. The strong blueshifted peak of the H_2CO emission is located $\sim 3''$ east of the protostar (Fig. 5), while the strong blueshifted CS emission peak is located $\sim 5''$ southwest (Wilner et al. 2000). If the blue asymmetry of the line profile was caused entirely by a bright clump in the outflowing gas, the strongest blueshifted emission should have come from the same part of the outflow. The difference between the H_2CO and the CS maps suggests that the outflow alone is not necessarily the dominating cause of the line profile asymmetry. Since most of the optically thick molecular lines of B335 show a blue-skewed line profile (Evans et al. 2005), the line asymmetry observed with single-dish telescopes is probably caused by a systematic effect, most likely the collapse, rather than the clumps in the outflow. Especially, the blue-skewed profiles of off-center spectra at positions in the north or south of the protostar (i.e., at positions in the direction perpendicular to the outflow) provide a strong evidence for infall motion (Zhou 1995; Choi et al. 1999).

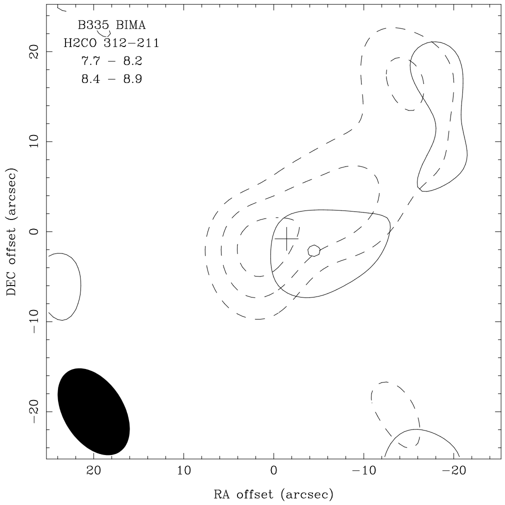

Fig. 5. Maps of the blueshifted (dashed contours) and the redshifted (solid contours) peaks of the H_2CO line. The H_2CO line intensity was averaged over the velocity intervals of $V_{\rm LSR}$ = (7.7, 8.2) and (8.4, 8.9) km s^{-1}, respectively. The contour levels are 1, 2, and 3 times 1.3 Jy $beam^{-1}$. The rms noise is 0.44 Jy $beam^{-1}$.

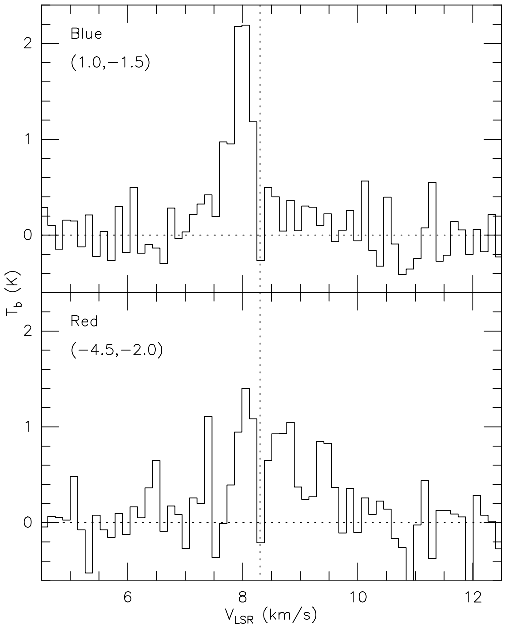

Fig. 6. Spectra of the H_2CO line at the maximum positions of the blueshifted (*top*) and the redshifted (*bottom*) emission. The position offset in arcseconds relative to the map center is written at the top left corner of each panel (see Fig. 5).

While the difference between the CS and the H_2CO maps may be caused by the chemical differentiation, the H_2CO and the CS maps have two features in common. First, the overall shape of the emission structure is elongated in the east-west direction, parallel to the outflow axis. Second, the blueshifted emission is either stronger than or comparable to the redshifted one in both the eastern and the western sides of the protostar. One possible explanation of these features may be the combined effect of the infalling envelope and the outflow on the radiative transfer (Fig. 7). If the outflow axis is nearly in the plane of the sky, and if the outflowing gas and the infalling gas along a single line of sight have comparable (projected) velocities, the emission from the redshifted outflowing gas can be absorbed by the redshifted infalling gas in the front hemisphere of the envelope. In contrast, the emission from the blueshifted envelope may not suffer from absorption if the blueshifted outflowing gas is optically thin and/or more highly excited. This effect can make the line profile asymmetry severer than what is expected from infall-only models. This model may not apply to every species/transitions because the infalling and the outflowing gas have quite different physical and chemical conditions. For example, the enhancement of gas-phase H_2CO and CS is expected in shocked outflowing gas while some molecules (such as DCO^+) are abundant only in the quiescent gas (for example, Bachiller & Pérez Gutiérrez 1997; Blake et al. 1995). Such an outflow-envelope coupling in radiative transfer may work for high-density tracer lines that are optically thin in the outflowing gas and moderately optically thick in the infalling envelope. For a better understanding and comparisons with observations, this model needs to be tested in detail using multi-dimensional radiative transfer codes.

We thank KASI ISMJC members for helpful discussions. This work was partially supported by the LRG Program of KASI.

References

André, P., Ward-Thompson, D., & Barsony, M. 1993, ApJ, 406, 122
Anglada, G., Rodriguez, L. F., Canto, J., Estalella, R., & Torrelles, J. M. 1992, ApJ, 395, 494
Bachiller, R., & Pérez Gutiérrez, M. 1997, APJ, 487, L93
Barnard, E. E., Frost, E. B., & Calvert, M. R. 1927, A Photographic Atlas of Selected Regions in the Milky Way (Washington: Carnegie Institute of Washington)
Beckwith, S. V. W., & Sargent, A. I. 1991, ApJ, 381, 250
Blake, G. A., Sandell, G., van Dishoeck, E. F., Groesbeck, T. D., Mundy, L. G., & Aspin, C. 1995, ApJ, 441, 689
Bok, B. J., Cordwell, C. S., & Cromwell, R. H. 1971, in Dark Nebulae, Globules and Protostars, ed B. T. Lynds (Tucson: Univ. Arizona Press), 33
Bok, B. J., & McCarthy, C. C. 1974, AJ, 79, 42
Cabrit, S., Goldsmith, P. F., & Snell, R. L. 1988, ApJ, 334, 196
Chandler, C. J., Gear, W. K., Sandell, G., Hayashi, S., Duncan, W. D., Griffin, M. J., & Hazella, S. 1990, MNRAS, 243, 330
Chandler, C. J., & Sargent, A. I. 1993, ApJ, 414, L29
Choi, M., Evans, N. J., II, Gregersen, E. M., & Wang, Y. 1995, ApJ, 448, 742
Choi, M., Panis, J.-F., & Evans, N. J., II 1999, ApJS, 122, 519
Evans, N. J., II, Lee, J.-E., Rawlings, J. M. C., & Choi, M. 2005, ApJ, 626, 919
Frerking, M. A., & Langer, W. D. 1982, ApJ, 256, 523
Frerking, M. A., Langer, W. D., & Wilson, R. W. 1987, ApJ, 313, 320
Gee, G., Griffin, M. J., Cunningham, T., Emerson, J. P., Ade, P. A. R., & Caroff, L. J. 1985, MNRAS, 215, 15P
Gregersen, E. M., Evans, N. J., II, Zhou, S., & Choi, M. 1997, ApJ, 484, 256
Harvey, D. W. A., Wilner, D. J., Lada, C. J., Myers, P. C., Alves, J. F., & Chen, H. 2001, ApJ, 563, 903
Harvey, D. W. A., Wilner, D. J., Myers, P. C., Tafalla, M., & Mardones, D. 2003a, ApJ, 583, 809
Harvey, D. W. A., Wilner, D. J., Myers, P. C., & Tafalla, M. 2003b, ApJ, 596, 383
Hirano, N., Kameya, O., Kasuga, T., & Umemoto, T. 1992, ApJ, 390, L85
Hirano, N., Kameya, O., Nakayama, M., & Takakubo, K. 1988, ApJ, 327, L69
Hodapp, K.-W. 1998, ApJ, 500, L183
Keene, J., Davidson, J. A., Harper, D. A., Hildebrand, R. H., Jaffe, D. T., Loewenstein, R. F., Low, F. J., & Pernic, R. 1983, ApJ, 274, L43
Martin, R. N., & Barrett, A. H. 1978, ApJS, 36, 1
Milman, A. S., Knapp, G. R., Knapp, S. L., & Wilson, W. J. 1975, AJ, 80, 101
Minn, Y. K., & Greenberg, J. M. 1973, A&A, 22, 13
Reipurth, B., Heathcote, S., & Vrba, F. 1992, A&A, 256, 225
Reipurth, B., Rodríguez, L. F., Anglada, G., & Bally, J. 2002, AJ, 124, 1045
Saito, M., Sunada, K., Kawabe, R., Kitamura, Y., & Hirano, N. 1999, ApJ, 518, 334
Shirley, Y. L., Evans, N. J., II, Rawlings, J. M. C., & Gregersen, E. M. 2000, ApJS, 131, 249
Takakuwa, S., Kamazaki, T., Saito, M., Yamaguchi, N., & Kohno, K. 2007, PASJ, 59, 1
Tomita, Y., Saito, T., & Ohtani, H. 1979, PASJ, 31, 407
Wilner, D. J., Myers, P. C., Mardones, D., & Tafalla, M. 2000, ApJ, 544, L69
Zhou, S. 1995, ApJ, 442, 685
Zhou, S., Evans, N. J., II, Butner, H. M., Kutner, M. L., Leung, C. M., & Mundy, L. G. 1990, ApJ, 363, 168
Zhou, S., Evans, N. J., II, Kömpe, C., & Walmsley, C. M. 1993, ApJ, 404, 232

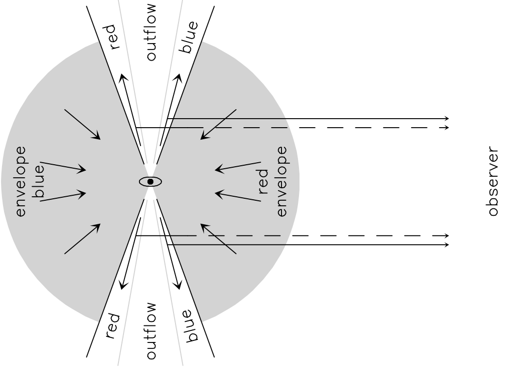

Fig. 7. Schematic diagram showing the effect of the infalling envelope (*gray sphere*) on the emission from the outflow. In this model, the outflow axis is nearly perpendicular to the line of sight, the outflowing gas is optically thin, and the infalling envelope is optically thick. Radiation from the redshifted outflow (*dashed line*) can be absorbed by the front part of the infalling envelope.